IEEE Access
Multidisciplinary | Rapid Review | Open Access Journal

Received September 10, 2021, accepted October 2, 2021, date of publication October 11, 2021, date of current version October 19, 2021.

Digital Object Identifier 10.1109/ACCESS.2021.3119396

Parameter Adaptive Control for a Quadrotor With a Suspended Unknown Payload Under External Disturbance

YING WU, YUN XIE, AND SEN LI
School of Automation, Guangdong University of Technology, Guangzhou 510006, China
Corresponding author: Yun Xie (xieyun@gdut.edu.cn)

This work was supported in part by the Natural Science Foundation of Guangdong Province under Grant 2016A030313706, and in part by the College Students' Innovative Entrepreneurial Training Plan Program of Guangdong Province, China, under Grant 201811845089.

ABSTRACT This paper focuses on the disturbance attenuation control of the quadrotor suspended payload system with unknown payload mass. Since the quadrotor transportation system is an eight-degree-of-freedom system with only four actuated degrees, it is difficult to achieve rapid stabilization of the quadrotor under varying payload and external disturbances. In this paper, a nonlinear controller based on rotation matrix is designed to rapid stabilization of attitude. By analyzing the effect of load mass on the trajectory tracking control, a parameter adaptive controller is proposed for position control. A mass estimation algorithm is established to estimate the payload mass in the air, which improves the robustness of the system. This approach can maximize load-bearing capacity within the thrust range of the quadrotor. The Lyapunov-based analysis proves the exponential convergence of the attitude error and the stability of the whole system. The contrast simulations demonstrate that the controller is superior to the sliding-mode controller incorporating input shaping on mass estimation, trajectory tracking, and disturbance resistance.

INDEX TERMS Adaptive control, disturbance attenuation, quadrotor, suspended payload.

I. INTRODUCTION

In recent years, Unmanned Aerial Vehicles (UAVs) have been widely studied and utilized in both military [1] and civilian [2] applications due to their simple structure and great maneuverability. With the deepening research on UAV flight control algorithms, the research hotspot of UAVs has gradually changed from attitude and position control to UAV applications such as UAV formation flight [3], fault-tolerant control [4], and load transportation control [5]. This leads to that the study of UAVs in spraying [6], surveillance [7], and fire rescue [8] field becomes more popular.

With the rapid development of the delivery industry, UAV logistics receive much attention [9]. UAV logistics is of great importance for courier delivery in remote and low-traffic areas. Zipline, a US company, has developed a high-safety, autonomous fixed-wing drone for aeromedical transportation. The company has saved many lives by transporting blood and medical supplies in Rwanda [10]. Research about UAV logistics includes drone lift [11], drone obstacle avoidance [12], collaborative drone robotic arm [13], [14], and drone trajectory tracking [15]. Among them, robustness to environmental disturbances and an unknown payload is necessary for UAV transportation applications. The quadrotor UAV is the simplest structure of vertical take-off and landing UAV, with algorithm universality. Therefore, this paper studies anti disturbance control of the quadrotor suspended payload system.

The quadrotor transportation system is an underactuated system with the high coupling of quadrotor position and payload swing angle. The payload oscillation also harms the position control of the payload transportation system [16]. So many studies have been done for stability control of the quadrotor transportation system [17]–[27]. Reference [17] designs a proportional plus derivative controller which will spend a lot of time to reach the balance point and have large steady-state error. In [25], a nonlinear controller is designed for the point-to-point flight which ensures the position error and swing angle converge exponentially to zero. However, the robustness of system against perturbations is not considered in these studies. Since the real environment is complex and changeable, the existence of external

The associate editor coordinating the review of this manuscript and approving it for publication was Bidyadhar Subudhi.

disturbance is inevitable. There are some studies to estimate and compensate the external disturbances [28]–[33]. Reference [28] presents a computational Geometric method to estimate the effects of wind. An uncertainty and disturbance estimator (UDE) is proposed in [30] for a quadrotor with a suspended payload. Though the uncertainty and disturbance estimator is suitable to attenuate unknown perturbations, it requires more computational power. And complex environment makes it very difficult to obtain an accurate model of external disturbance. Hence, the controller with high robustness is more appropriate for disturbance rejection control of the quadrotor transportation system. The adaptive control methods in both [34] and [35] show that the quadrotor's states can be stabilized in finite time when facing external disturbance.

The payloads with unknown masses are also a challenge of the stable fight. Indeed, only a few literatures investigated stable control of quadrotor with an unknown payload mass [36]–[38]. A linear Proportional-Integral-Derivative controller is designed to probe the effect of a helicopter under the disturbance of increased payload mass in [36]. Under this control method, a helicopter can reduce added load offsets within a relatively large range. And successful helicopter loading deployments are not susceptible to substantial changes in mass. Unlike external disturbances, the payload mass change is relatively small or unchanged. Therefore, mass estimation is more suited to stable control of the quadrotor transportation system than the robust controller. For the variable load, [37] proposed a mass estimation algorithm to estimate the quadrotor mass in the air. Combining with a novel robust sliding mode, the mass estimation algorithm can improve the quadrotor's performance in suppressing the variable payload disturbance. Reference [38] presents a fixed-gain nonlinear proportional-derivative controller to meet the expected performance for an effective payload mass and a retrospective cost adaptive controller to compensate for the uncertain payload mass. However, due to the complicated nonlinear model of the quadrotor with a suspended payload, it is difficult to estimate the payload mass in the air. To the best knowledge of the authors, few previous works have achieved mass estimation of a quadrotor with a suspended payload.

In this paper, the quadrotor transportation system is modeled based on the Lagrange equation, and the influence of the payload mass on the trajectory tracking control performance is explored through the analysis of the model. The proposed controller is divided into three parts: attitude control, position control, and oscillation suppression. A nonlinear attitude controller based on a rotation matrix and feedback is designed. However, the position control and the oscillation suppression of the quadrotor are coupled together. Therefore, we designed a nonlinear control method and a mass estimation algorithm, which can adjust the control parameters based on the mass of the payload. By Lyapunov stability theory analysis, the system can be shown to be exponentially stable in attitude, with the convergence of both position error and payload swing angle. By the performance analysis method proposed in [24], the simulation results show that the proposed trajectory tracking controller is effective in improving robustness to external disturbance and unknown payload mass. Besides, payload mass can be accurately estimated and the maximum load mass can reach 1 kg. The main contributions of this work are as follows:

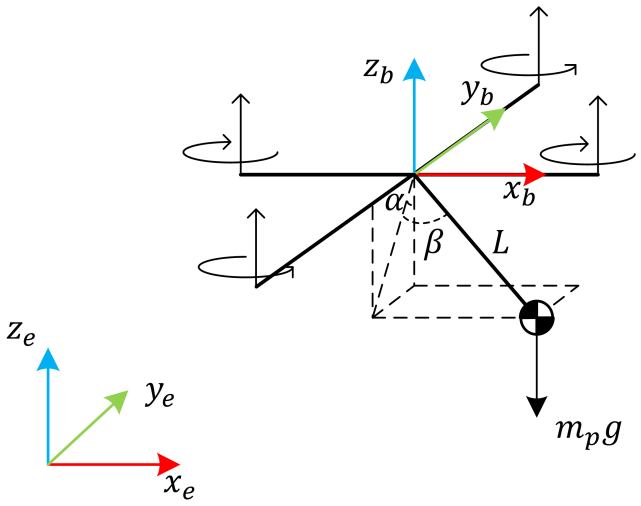

FIGURE 1. Quadrotor with suspended load.

1) A mass estimation algorithm is designed for a quadrotor with a suspended payload, which is proven to be able to precisely estimate the payload mass of a quadrotor transportation system in the air.
2) A novel parameter adaptive control law is proposed, which is combined with the estimated payload mass and state feedback to improve the robustness of the traditional adaptive control law. The proposed trajectory tracking controller can enhance the trajectory tracking control performance and increase the maximum payload capacity under external disturbances.

This paper is organized as follows. The dynamics of the quadrotor with a slung payload is demonstrated in Section II. Section III details the design of attitude controller, position controller, and swing suppression. The simulation results are analyzed in Section IV. Finally, concluding remarks are provided in Section V.

II. MODEL

This section introduces the nonlinear model of the quadrotor with a suspended load derived by Lagrange's equation. The quadrotor transportation system, the inertial coordinate frame $\{x_e y_e z_e\}$, and the body-fixed coordinate frame $\{x_b y_b z_b\}$ are shown in Fig. 1. And the body-fixed coordinate frame is fixed to the mass center of the quadrotor.

A. NOTATION

In this paper, $\mathbb{R}^{m\times n}$ represents the $m \times n$ dimensional real vector space. $||*||$ is the Euclidean norm of $* \in \mathbb{R}^n$. The symbols c_* and s_* denote $\cos(*)$ and $\sin(*)$, respectively.

TABLE 1. Symbol summary.

Symbol	Description
$\boldsymbol{p}_l = \begin{bmatrix} p_{lx} & p_{ly} & p_{lz} \end{bmatrix}^T \in \mathbb{R}^3$	position of the payload
$\boldsymbol{p}_q = \begin{bmatrix} p_{qx} & p_{qy} & p_{qz} \end{bmatrix}^T \in \mathbb{R}^3$	position of the quadrotor
$\boldsymbol{\gamma} = \begin{bmatrix} \alpha & \beta \end{bmatrix}^T \in \mathbb{R}^2$	swing angle of the payload
$L \in \mathbb{R}$	length of the cable
$\boldsymbol{J} \in \mathbb{R}^{3\times3}$	inertia matrix of the quadrotor
$\boldsymbol{R} \in \mathbb{R}^{3\times3}$	rotation matrix of quadrotor attitude
$\boldsymbol{\Omega} \in \mathbb{R}^3$	the body angular velocity
$\boldsymbol{\tau} \in \mathbb{R}^3$	torque of the four rotors
$f \in \mathbb{R}$	total thrust of the four rotors
$\boldsymbol{I}_n \in \mathbb{R}^n$	n-dimensional identity matrix
$\boldsymbol{0}_{m\times n} \in \mathbb{R}^{m\times n}$	$m \times n$ dimensional null matrix
$m_q \in \mathbb{R}$	the quadrotor mass
$m_p \in \mathbb{R}$	the payload mass
$\boldsymbol{G} = \begin{bmatrix} 0 & 0 & g \end{bmatrix}^T \in \mathbb{R}^3$	the gravitational acceleration

$\boldsymbol{y} = diag(\boldsymbol{x}) \in \mathbb{R}^{n\times n}$ is a diagonal matrix whose N^{th} diagonal element is the N^{th} element of vector $\boldsymbol{x} \in \mathbb{R}^n$. The "wedge" operator produces a skew-symmetric matrix which satisfies $\hat{\boldsymbol{a}}\boldsymbol{b} = \boldsymbol{a} \times \boldsymbol{b}$ for $\forall\, \boldsymbol{a}, \boldsymbol{b} \in \mathbb{R}^3$. And " vee" operator $(*)^\vee$ is the inverse operator of the "wedge" operator. The symbols used in the paper are summarized in Table 1.

B. SYSTEM DYNAMICS

The motion equation of our cargo transportation system is derived from the following assumptions.

- Assumption 1: The payload is connected to the mass center of the quadrotor through a cable.
- Assumption 2: The position of quadrotor is always above the payload.
- Assumption 3: The cable connecting the quadrotor to the payload is inelastic, weightless, and always taut.

From Fig. 1, the position of the load is given by the following equations.

$$\boldsymbol{p}_l = \boldsymbol{p}_q + \boldsymbol{p}_l^b \tag{1}$$

$$\boldsymbol{p}_l^b = \begin{bmatrix} L\sin\beta & -L\cos\beta\sin\alpha & -L\cos\beta\cos\alpha \end{bmatrix}^T \tag{2}$$

The quadrotor suspended payload system is segmented in the quadrotor attitude subsystem, the quadrotor position subsystem, and slung payload subsystem. The quadrotor position subsystem and slung payload subsystem influence each other. Since the dynamic model of our cargo transportation system is more complex than the quadrotor dynamic model, we obtain the motion equation via Lagrange's equation. The derivation of our system model considers only gravity and the thrust provided by the propellers. The Lagrange's equation is given by:

$$\frac{d}{dt}\frac{\partial L}{\partial \dot{\boldsymbol{q}}(i)} - \frac{\partial L}{\partial \boldsymbol{q}(i)} = \bar{\boldsymbol{F}}(i) \tag{3}$$

Therefore, the Lagrangian can be taken as $L = T(\boldsymbol{q}, \dot{\boldsymbol{q}}) - V(\boldsymbol{q}, \dot{\boldsymbol{q}})$ where T and V are the translational kinetic energy and potential energy of the system, respectively. The generalized coordinates include the quadrotor's position and the slung load's swing angle. Defining three unit orthogonal vectors as $\boldsymbol{p}_1 = \begin{bmatrix} s_\beta & -c_\beta s_\alpha & -c_\beta c_\alpha \end{bmatrix}^T$, $\boldsymbol{p}_2 = \begin{bmatrix} 0 & c_\alpha & -s_\alpha \end{bmatrix}^T$, and $\boldsymbol{p}_3 = \begin{bmatrix} -c_\beta & -s_\alpha s_\beta & -s_\alpha s_\alpha \end{bmatrix}^T$, the motion equation of the system is given by:

$$\ddot{\boldsymbol{q}} = \boldsymbol{M}(\boldsymbol{q})\bar{\boldsymbol{F}} + \boldsymbol{C}(\boldsymbol{q}, \dot{\boldsymbol{q}}) \tag{4}$$

$$\boldsymbol{\tau} = \boldsymbol{J}\dot{\boldsymbol{\Omega}} + \boldsymbol{\Omega} \times \boldsymbol{J}\boldsymbol{\Omega} \tag{5}$$

$$\dot{\boldsymbol{q}} = \dot{\boldsymbol{q}} \tag{6}$$

$$\dot{\boldsymbol{R}} = \boldsymbol{R}\hat{\boldsymbol{\Omega}} \tag{7}$$

where $\boldsymbol{q} = \begin{bmatrix} \boldsymbol{p}_q^T & \boldsymbol{\gamma}^T \end{bmatrix}^T \in \mathbb{R}^5$, $\bar{\boldsymbol{F}} = \begin{bmatrix} \boldsymbol{F}^T & \boldsymbol{0}_{2\times1}^T \end{bmatrix}^T \in \mathbb{R}^5$, and $\boldsymbol{F} = \boldsymbol{R}\begin{bmatrix} 0 & 0 & f \end{bmatrix}^T \in \mathbb{R}^3$. The matrix in (4) is defined as:

$$\boldsymbol{M}(\boldsymbol{q}) = \begin{bmatrix} \boldsymbol{M}_{11} & \boldsymbol{0}_{3\times2} \\ \boldsymbol{0}_{2\times3} & \boldsymbol{M}_{22} \end{bmatrix} \tag{8}$$

$$\boldsymbol{C}(\boldsymbol{q}, \dot{\boldsymbol{q}}) = \begin{bmatrix} \boldsymbol{C}_1(\boldsymbol{q}, \dot{\boldsymbol{q}}) \\ \boldsymbol{C}_2(\boldsymbol{q}, \dot{\boldsymbol{q}}) \end{bmatrix} \tag{9}$$

$$\boldsymbol{M}_{11} = \frac{1}{m_q}(\boldsymbol{I}_3 - \frac{m_p}{m_q + m_p}\boldsymbol{p}_1\boldsymbol{p}_1^T) \tag{10}$$

$$\boldsymbol{M}_{22} = \frac{1}{m_q L}\begin{bmatrix} \frac{1}{c_\beta}\boldsymbol{p}_2 & \boldsymbol{p}_3 \end{bmatrix}^T \tag{11}$$

$$\boldsymbol{C}_1(\dot{\boldsymbol{q}}, \ddot{\boldsymbol{q}}) = \frac{m_p L c_\beta^2 \dot{\alpha}^2}{m_q + m_p}\boldsymbol{p}_1 - \boldsymbol{G} \tag{12}$$

$$\boldsymbol{C}_2(\dot{\boldsymbol{q}}, \ddot{\boldsymbol{q}}) = \begin{bmatrix} \frac{2\dot{\alpha}\dot{\beta}s_\beta}{c_\beta} & -c_\beta s_\alpha \dot{\alpha}^2 \end{bmatrix}^T. \tag{13}$$

Therefore, (4) can be transformed into the following equations after some mathematical operations.

$$\ddot{\boldsymbol{p}}_q = \frac{1}{m_q}(\boldsymbol{I}_3 - \frac{m_p}{m_q + m_p}\boldsymbol{p}_1\boldsymbol{p}_1^T)\boldsymbol{F} + \boldsymbol{C}_1 \tag{14}$$

$$\ddot{\boldsymbol{\gamma}} = \frac{1}{m_q L}\begin{bmatrix} \frac{1}{c_\beta}\boldsymbol{p}_2^T \\ \boldsymbol{p}_3^T \end{bmatrix}\boldsymbol{F} + \boldsymbol{C}_2 \tag{15}$$

From (14), the dynamic model of the quadrotor transportation system is affected by the payload mass and the payload swing angle. And the greater the scale of the payload mass to the quadrotor mass, the more the quadrotor position is greatly influenced by the load swing.

III. CONTROL DESIGN

In this section, a parameter adaptive controller is presented to enhance the performance of the tracking control in the face of large unknown payload mass and environmental disturbance. The architecture diagram of the parameter adaptive controller is illustrated in Fig. 2.

A. ATTITUDE CONTROL

Denote the rotation matrix representing the desired attitude of the quadrotor as $\boldsymbol{R}_d$. Then the attitude error matrix of the quadrotor is defined as:

$$\boldsymbol{R}_e = \boldsymbol{R}^T\boldsymbol{R}_d \tag{16}$$

where the error rotation matrix can be expressed as:

$$\boldsymbol{R}_e = \exp(\hat{\boldsymbol{\Omega}}_e\theta) = \boldsymbol{I} + \hat{\boldsymbol{\Omega}}_e sin\theta + \hat{\boldsymbol{\Omega}}_e^2(1 - cos\theta). \tag{17}$$

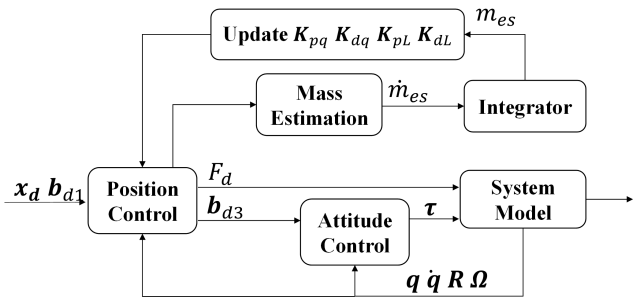

FIGURE 2. Architecture diagram of the parameter adaptive controller.

The above equation and the ''vee'' operator translate the error rotation matrix into an error vector representing the attitude error of the quadrotor.

$$\boldsymbol{e}_R = \log\left(\boldsymbol{R}_e\right)^{\vee} = \boldsymbol{\Omega}_e\theta \tag{18}$$

Therefore, the angular velocity error of the body is defined as:

$$\boldsymbol{e}_\Omega = \dot{\boldsymbol{e}}_R = \boldsymbol{\Omega}_d - \boldsymbol{\Omega} \tag{19}$$

where $\boldsymbol{\Omega}_d$ is the desired angular velocity. From (19), the attitude error dynamics is

$$\boldsymbol{J}\dot{\boldsymbol{e}}_\Omega = \boldsymbol{J}\dot{\boldsymbol{\Omega}}_d - \boldsymbol{J}\dot{\boldsymbol{\Omega}}. \tag{20}$$

Theorem 1: Considering the desired attitude, desired angular velocity, and desired angular acceleration are known and bounded, the control torque is designed as

$$\boldsymbol{\tau} = \boldsymbol{K}_R\boldsymbol{e}_R + \boldsymbol{K}_\Omega\boldsymbol{e}_\Omega + \boldsymbol{J}\dot{\boldsymbol{\Omega}}_d + \boldsymbol{\Omega}\times\boldsymbol{J}\boldsymbol{\Omega} \tag{21}$$

where $\boldsymbol{K}_R = diag(\begin{bmatrix}K_{Rx} & K_{Ry} & K_{Rz}\end{bmatrix}) \in \mathbb{R}^{3\times3}$ and $\boldsymbol{K}_\Omega = diag(\begin{bmatrix}K_{\Omega x} & K_{\Omega y} & K_{\Omega z}\end{bmatrix}) \in \mathbb{R}^{3\times3}$. Then the attitude error and angular velocity error are globally exponentially stable at $\boldsymbol{R}_e = \boldsymbol{I}_3$ and $\boldsymbol{e}_\Omega = \begin{bmatrix}0 & 0 & 0\end{bmatrix}$.

Proof: Consider the Lyapunov function as

$$V_1 = \boldsymbol{e}_R^T\boldsymbol{K}_R\boldsymbol{e}_R + \boldsymbol{e}_\Omega^T\boldsymbol{J}\boldsymbol{e}_\Omega. \tag{22}$$

Then the derivative of $\dot{V}_1$ is

$$\dot{V}_1 = \boldsymbol{e}_R^T\boldsymbol{K}_R\dot{\boldsymbol{e}}_R + \boldsymbol{e}_\Omega^T\boldsymbol{J}\dot{\boldsymbol{e}}_\Omega. \tag{23}$$

Substituting (5) and (21) for (20), the attitude error dynamic becomes

$$\boldsymbol{J}\dot{\boldsymbol{e}}_\Omega = -\boldsymbol{K}_R\boldsymbol{e}_R - \boldsymbol{K}_\Omega\boldsymbol{e}_\Omega. \tag{24}$$

Therefore, the derivative of V is

$$\dot{V}_1 = -\boldsymbol{e}_\Omega^T\boldsymbol{K}_\Omega\boldsymbol{e}_\Omega \le 0. \tag{25}$$

Since the Lyapunov function is bounded, while the rotation matrix group is compact, then $\boldsymbol{e}_R$ and $\boldsymbol{e}_\Omega$ are bounded. The derivative of $\dot{V}_1$ is

$$\ddot{V}_1 = -\boldsymbol{e}_\Omega^T\boldsymbol{K}_\Omega\boldsymbol{J}^{-1}(-\boldsymbol{K}_R\boldsymbol{e}_R - \boldsymbol{K}_\Omega\boldsymbol{e}_\Omega). \tag{26}$$

Since all signals on the right-hand side of (26) are bounded, $\ddot{V}_1$ is bounded. While the $\dot{V}_1$ is uniformly continuous, $\dot{V}_1$ converges to zero applying Barbalat's lemma. Therefore $\boldsymbol{e}_\Omega$ is globally asymptotically stable to the equilibrium point zero. The derivative of $\dot{\boldsymbol{e}}_\Omega$ is

$$\boldsymbol{J}\ddot{\boldsymbol{e}}_\Omega = -\boldsymbol{K}_R\boldsymbol{e}_\Omega - \boldsymbol{K}_\Omega\dot{\boldsymbol{e}}_\Omega. \tag{27}$$

Since all signals on the right-hand side of (27) are bounded and $\dot{\boldsymbol{e}}_\Omega$ is uniformly continuous, $\dot{\boldsymbol{e}}_\Omega$ converges to zero applying Barbalat's lemma. Therefore $\dot{\boldsymbol{e}}_\Omega$ is globally asymptotically stable to the equilibrium point zero. The (24) can be rewritten as

$$\boldsymbol{K}_R\boldsymbol{e}_R = -\boldsymbol{K}_\Omega\boldsymbol{e}_\Omega - \boldsymbol{J}\dot{\boldsymbol{e}}_\Omega. \tag{28}$$

Therefore,

$$\|\boldsymbol{K}_R\boldsymbol{e}_R\| = \|-\boldsymbol{K}_\Omega\boldsymbol{e}_\Omega - \boldsymbol{J}\dot{\boldsymbol{e}}_\Omega\| \le \|\boldsymbol{K}_\Omega\boldsymbol{e}_\Omega\| + \|\boldsymbol{J}\dot{\boldsymbol{e}}_\Omega\|. \tag{29}$$

Since $\|\boldsymbol{K}_\Omega\boldsymbol{e}_\Omega\| \to 0$ and $\|\boldsymbol{J}\dot{\boldsymbol{e}}_\Omega\| \to 0$, it follows that $\|\boldsymbol{K}_R\boldsymbol{e}_R\| \to 0$. Then the attitude error system is globally asymptotically stable.

To prove globally exponential stability, we define $\boldsymbol{q}_1 = \begin{bmatrix}\boldsymbol{e}_R^T & \boldsymbol{e}_\Omega^T\end{bmatrix}^T$. Equation (22) can be rewritten as

$$V_1 = \boldsymbol{q}_1^T\boldsymbol{P}_1\boldsymbol{q}_1 \tag{30}$$

where

$$\boldsymbol{P}_1 = \begin{bmatrix}\boldsymbol{K}_R & 0\\ 0 & \boldsymbol{J}\end{bmatrix}. \tag{31}$$

It follows that $\lambda_{min}\left\|\boldsymbol{q}_1\right\|^2 \le V_1 \le \lambda_{max}\left\|\boldsymbol{q}_1\right\|^2$ where λ_{max} and λ_{min} are the maximum eigenvalue and the minimum eigenvalue of $\boldsymbol{P}_1$. λ_Ω is the minimum eigenvalue of $\boldsymbol{K}_\Omega$. Then $\dot{V}_1$ satisfies the following inequality.

$$\dot{V}_1 =\le -\lambda_\Omega\left\|\boldsymbol{q}_1\right\|^2 \le -\frac{\lambda_\Omega}{\lambda_{max}}V_1 \tag{32}$$

Base on the upper of V_1 is derived as

$$V_1 \le V_1(0)\exp(-\frac{\lambda_\Omega}{\lambda_{max}}t). \tag{33}$$

It can be concluded that

$$\left\|\boldsymbol{q}_1\right\| \le \sqrt{\frac{\lambda_{max}}{\lambda_{min}}}\left\|\boldsymbol{q}_1(0)\right\|\exp(-\frac{\lambda_\Omega}{2\lambda_{max}}t). \tag{34}$$

Hence, the attitude error system is globally exponential stability.

B. POSITION CONTROL

Denote the desired position of the quadrotor as $\boldsymbol{p}_d$. The position error and velocity error of the quadrotor are defined as

$$\boldsymbol{e}_p = \boldsymbol{p}_q - \boldsymbol{p}_d \tag{35}$$

$$\dot{\boldsymbol{e}}_p = \dot{\boldsymbol{p}}_q - \dot{\boldsymbol{p}}_d. \tag{36}$$

Therefore, the position error dynamics and the payload's swing angle dynamics are derived as

$$\ddot{\boldsymbol{e}}_p = \boldsymbol{\omega}_q + \boldsymbol{g}_q\boldsymbol{F} \tag{37}$$

$$\ddot{\boldsymbol{\gamma}} = \boldsymbol{\omega}_L + \boldsymbol{g}_L \boldsymbol{F}. \tag{38}$$

where $\boldsymbol{g}_q$, $\boldsymbol{\omega}_q$, $\boldsymbol{g}_L$, and $\boldsymbol{\omega}_L$ in (37) and (38) are

$$\boldsymbol{g}_q = \frac{1}{m_q}(\boldsymbol{I}_3 - \frac{m_p}{m_q + m_p}\boldsymbol{p}_1\boldsymbol{p}_1^T) \tag{39}$$

$$\boldsymbol{\omega}_q = \frac{m_p L c_\beta^2 \dot{\alpha}^2}{m_q + m_p}\boldsymbol{p}_1 - \boldsymbol{G} - \ddot{\boldsymbol{p}}_d \tag{40}$$

$$\boldsymbol{g}_L = \frac{1}{m_q L}\begin{bmatrix} \frac{1}{c_\beta}\boldsymbol{p}_2^T \\ \boldsymbol{p}_3^T \end{bmatrix} \tag{41}$$

$$\boldsymbol{\omega}_L = \begin{bmatrix} \frac{2\dot{\alpha}\dot{\beta}s_\beta}{c_\beta} & -c_\beta s_\alpha \dot{\alpha}^2 \end{bmatrix}^T. \tag{42}$$

First, consider the desired thrust as

$$\boldsymbol{F}_d = f\boldsymbol{R}_d\,[0,\,0,\,1]^T. \tag{43}$$

We denote the control input f as

$$\boldsymbol{F} = f\boldsymbol{R}_d\,[0,\,0,\,1]^T + \boldsymbol{\kappa} f. \tag{44}$$

Then we take $\boldsymbol{b}_3$ to be the third column vector of $\boldsymbol{R}$ and $\boldsymbol{b}_{d3}$ to be the third column vector of $\boldsymbol{R}_d$. While θ_3 is the variation of the angle between the vector $\boldsymbol{b}_3$ and the vector $\boldsymbol{b}_{d3}$, it follows that

$$\boldsymbol{\kappa} = (\boldsymbol{b}_3 - \boldsymbol{b}_{d3}) \tag{45}$$

$$\|\boldsymbol{b}_3 - \boldsymbol{b}_{d3}\| < |\theta_3| \leq \|\boldsymbol{e}_R\|. \tag{46}$$

Based (45) and (46), we can conclude that

$$\|\kappa\| \leq \|\boldsymbol{e}_R\|. \tag{47}$$

Equation (37) and (38) are formatted as

$$\ddot{\boldsymbol{e}}_p = \boldsymbol{g}_q\boldsymbol{F}_d + \boldsymbol{\omega}_q + \boldsymbol{g}_q\boldsymbol{\kappa} f \tag{48}$$

$$\ddot{\boldsymbol{\gamma}} = \boldsymbol{g}_L\boldsymbol{F}_d + \boldsymbol{\omega}_L + \boldsymbol{g}_L\boldsymbol{\kappa} f. \tag{49}$$

The desired control thrust is designed as

$$\boldsymbol{F}_d = \boldsymbol{g}_q^{-1}(-\boldsymbol{\omega}_q + \boldsymbol{u}_q + L[\boldsymbol{p}_2 c_\beta, \boldsymbol{p}_3]\boldsymbol{u}_L) \tag{50}$$

where $\boldsymbol{u}_q$ and $\boldsymbol{u}_L$ are designed for the position control and payload swing suppression. $\boldsymbol{g}_q^{-1}$ is calculated as

$$\boldsymbol{g}_q^{-1} = m_{es}(\boldsymbol{I}_3 + \frac{m_p}{m_{es}}\boldsymbol{p}_1\boldsymbol{p}_1^T). \tag{51}$$

And based on (50), the desired attitude rotation matrix is calculated as

$$\boldsymbol{R}_d = [\boldsymbol{b'}_{1d} \quad \boldsymbol{b}_{2d} \quad \boldsymbol{b}_{3d}] \tag{52}$$

where $\boldsymbol{b}_{3d} = \frac{\boldsymbol{F}_d}{\|\boldsymbol{F}_d\|}$, $\boldsymbol{b}_{2d} = \boldsymbol{b}_{3d} \times \boldsymbol{b}_{1d}$, and $\boldsymbol{b'}_{1d} = \boldsymbol{b}_{2d} \times \boldsymbol{b}_{3d}$.

It is assumed that the estimated payload mass is equal to the actual payload mass. Since $\boldsymbol{p}_1, \boldsymbol{p}_2$, and $\boldsymbol{p}_3$ are orthogonal to each other, substituting (50) into (48) and (49) yields

$$\ddot{\boldsymbol{e}}_p = \boldsymbol{u}_q + L[c_\beta\boldsymbol{p}_2, \boldsymbol{p}_3]\boldsymbol{u}_L + \boldsymbol{g}_q\boldsymbol{\kappa} f \tag{53}$$

$$\ddot{\boldsymbol{\gamma}} = -\boldsymbol{g}_L\boldsymbol{g}_q^{-1}\boldsymbol{\omega}_q + \boldsymbol{g}_L\boldsymbol{g}_q^{-1}\boldsymbol{u}_q + \boldsymbol{u}_L + \boldsymbol{\omega}_L + \boldsymbol{g}_L\boldsymbol{\kappa} f. \tag{54}$$

Denoting $\boldsymbol{\Gamma}(\boldsymbol{\gamma}, \dot{\boldsymbol{\gamma}}) = \boldsymbol{\omega}_L - \boldsymbol{g}_L\boldsymbol{g}_q^{-1}\boldsymbol{\omega}_q + \frac{g}{L}\boldsymbol{\gamma}$, the position error dynamics and the payload's swing angle dynamics are formatted as

$$\ddot{\boldsymbol{e}}_p = \boldsymbol{u}_q + L[\boldsymbol{e}_2, \boldsymbol{e}_3]\boldsymbol{u}_L + \boldsymbol{h}_q + \boldsymbol{\kappa}_q \tag{55}$$

$$\ddot{\boldsymbol{\gamma}} = \boldsymbol{u}_L - \frac{g}{L}\boldsymbol{\gamma} + \frac{1}{L}\begin{bmatrix} \boldsymbol{e}_2^T \\ \boldsymbol{e}_3^T \end{bmatrix}\boldsymbol{u}_q + \boldsymbol{h}_L + \boldsymbol{\kappa}_L. \tag{56}$$

with unit vectors $\boldsymbol{e}_1 = \begin{bmatrix}0\ 0\ -1\end{bmatrix}^T$, $\boldsymbol{e}_2 = \begin{bmatrix}0\ 1\ 0\end{bmatrix}^T$, and $\boldsymbol{e}_3 = \begin{bmatrix}-1\ 0\ 0\end{bmatrix}$. And the functions defined in (55) and (56) are

$$\boldsymbol{h_q} = L\bar{\boldsymbol{h}}_q\boldsymbol{u_L} \tag{57}$$

$$\boldsymbol{\kappa}_q = \boldsymbol{g}_q\boldsymbol{\kappa} f \tag{58}$$

$$\boldsymbol{h}_L = \frac{1}{L}\bar{\boldsymbol{h}}_L\boldsymbol{u}_q + \boldsymbol{\Gamma} \tag{59}$$

$$\boldsymbol{\kappa}_L = \boldsymbol{g}_L\boldsymbol{\kappa} f \tag{60}$$

$$\bar{\boldsymbol{h}}_q = [c_\beta\boldsymbol{p}_2 - \boldsymbol{e}_2, \boldsymbol{p}_3 - \boldsymbol{e}_3] \tag{61}$$

$$\bar{\boldsymbol{h}}_L = \begin{bmatrix} \frac{1}{c_\beta}\boldsymbol{p}_2^T - \boldsymbol{e}_2^T \\ \boldsymbol{p}_3^T - \boldsymbol{e}_3^T \end{bmatrix}. \tag{62}$$

Based on assumption 2, there exist constants $\rho_q > 0$ and $\rho_L > 0$ satisfying the inequalities $\|\bar{\boldsymbol{h}}_q\| < \rho_q\|\boldsymbol{\gamma}\|$ and $\|\bar{\boldsymbol{h}}_L\| < \rho_L\|\boldsymbol{\gamma}\|$. Since $\|\boldsymbol{p}_1\| = 1$, $\|\boldsymbol{p}_2\| = 1$, and $\|\boldsymbol{p}_3\| = 1$, it can be concluded that

$$\|\boldsymbol{g}_q\| \leq \frac{1}{m_q}(\|\boldsymbol{I}_3\| + \|\frac{m_p}{m_q + m_p}\boldsymbol{p}_1\boldsymbol{p}_1^T\|) \leq \bar{g}_q \tag{63}$$

$$\|\boldsymbol{g}_L\| = \frac{1}{m_q L}\|\begin{bmatrix} \frac{1}{c_\beta}\boldsymbol{p}_2^T \\ \boldsymbol{p}_3^T \end{bmatrix}\| \leq \bar{g}_L. \tag{64}$$

where $\bar{g}_q$ and $\bar{g}_L$ are two positive constants. Considering $\boldsymbol{q}_\gamma = [\boldsymbol{\gamma}^T, \dot{\boldsymbol{\gamma}}^T]^T$, $\|\boldsymbol{\Gamma}\|$ is upper bounded as

$$\|\boldsymbol{\Gamma}\| \leq \bar{\rho}_\gamma(\ddot{\boldsymbol{p}}_q) + \rho_\gamma(\ddot{\boldsymbol{p}}_q)\|\boldsymbol{q}_\gamma\|^2 \tag{65}$$

with two constants $\rho_\gamma(\ddot{\boldsymbol{p}}_q) > 0$ and $\bar{\rho}_\gamma(\ddot{\boldsymbol{p}}_q) > 0$. The above analysis can be concluded that

$$\begin{cases} \|\boldsymbol{h}_q\| & \leq L\rho_q\|\boldsymbol{\gamma}\|\|\boldsymbol{u}_L\| \\ \|\boldsymbol{\kappa}_q\| & \leq \bar{g}_q\|\boldsymbol{e}_R\|f \\ \|\boldsymbol{h}_L\| & \leq \frac{1}{L}\rho_L\|\boldsymbol{\gamma}\|\|\boldsymbol{u}_q\| + \bar{\rho}_\gamma(\ddot{\boldsymbol{p}}_d) + \rho_\gamma(\ddot{\boldsymbol{p}}_d)\|\boldsymbol{q}_\gamma\|^2 \\ \|\boldsymbol{\kappa}_L\| & \leq \bar{g}_L\|\boldsymbol{e}_R\|f. \end{cases} \tag{66}$$

By analyzing the error dynamics of (14) and (15), the adaptive control law $\boldsymbol{u}_q$ and $\boldsymbol{u}_L$ are designed as:

$$\boldsymbol{u}_q = -\boldsymbol{K}_{pq}(m_{es})\boldsymbol{e}_p - \boldsymbol{K}_{dq}(m_{es})\dot{\boldsymbol{e}}_p \tag{67}$$

$$\boldsymbol{u}_L = -\boldsymbol{K}_{pL}(m_{es})\boldsymbol{e}_L - \boldsymbol{K}_{dL}(m_{es})\dot{\boldsymbol{e}}_L \tag{68}$$

where $\boldsymbol{K}_{pq}(m_{es}) = diag(\begin{bmatrix}K_{pqx} & K_{pqy} & K_{pqz}\end{bmatrix}) \in \mathbb{R}^{3\times3}$, $\boldsymbol{K}_{dq}(m_{es}) = diag(\begin{bmatrix}K_{dqx} & K_{dqy} & K_{dqz}\end{bmatrix}) \in \mathbb{R}^{3\times3}$, $\boldsymbol{K}_{pL}(m_{es}) = diag(\begin{bmatrix}K_{pLx} & K_{pLy}\end{bmatrix}) \in \mathbb{R}^{2\times2}$, and $\boldsymbol{K}_{dL}(m_{es}) = diag(\begin{bmatrix}K_{dLx} & K_{dLy}\end{bmatrix}) \in \mathbb{R}^{2\times2}$. And the mass estimation algorithm is defined as:

$$\dot{m}_{es} = -k_m\boldsymbol{u}_q(3). \tag{69}$$

The closed-loop dynamics of (55) and (56) is formatted as

$$\dot{\boldsymbol{q}}_2 = \boldsymbol{A}_2\boldsymbol{q}_2 + \boldsymbol{\kappa}_2 + \boldsymbol{h}_2. \tag{70}$$

In (70), the vector $\boldsymbol{q}_2 = [\boldsymbol{e}_p^T, \dot{\boldsymbol{e}}_p^T, \boldsymbol{q}_\gamma^T]^T$ represents the state of the closed-loop system, and the matrix $\boldsymbol{A_2}$ is

$$\boldsymbol{A_2} = \begin{bmatrix} \boldsymbol{0}_{3\times3} & \boldsymbol{I}_3 & \boldsymbol{0}_{3\times2} & \boldsymbol{0}_{3\times2} \\ -\boldsymbol{K}_{pq} & -\boldsymbol{K}_{dq} & L\boldsymbol{e}_{23}\boldsymbol{K}_{pL} & L\boldsymbol{e}_{23}\boldsymbol{K}_{dL} \\ \boldsymbol{0}_{2\times3} & \boldsymbol{0}_{2\times3} & \boldsymbol{0}_{2\times2} & \boldsymbol{I}_2 \\ \dfrac{\boldsymbol{e}_{23}^T\boldsymbol{K}_{pq}}{L} & \dfrac{\boldsymbol{e}_{23}^T\boldsymbol{K}_{dq}}{L} & \boldsymbol{A}_2' & -\boldsymbol{K}_{dL} \end{bmatrix} \tag{71}$$

where $\boldsymbol{e_{23}} = \begin{bmatrix}\boldsymbol{e_2}\ \boldsymbol{e_3}\end{bmatrix}$, $\boldsymbol{A}_2' = -\boldsymbol{K}_{pL} - \frac{g}{L}\boldsymbol{I}_2 \in \mathbb{R}^{2\times2}$, $\boldsymbol{\kappa}_2 = \begin{bmatrix}\boldsymbol{0}_{3\times1}^T\ \boldsymbol{\kappa}_q^T\ \boldsymbol{0}_{2\times1}^T\ \boldsymbol{\kappa}_L^T\end{bmatrix}^T$, and $\boldsymbol{h}_2 = \begin{bmatrix}\boldsymbol{0}_{3\times1}^T\ \boldsymbol{h}_q^T\ \boldsymbol{0}_{2\times1}^T\ \boldsymbol{h}_L^T\end{bmatrix}^T$. It is not hard to conclude that $\boldsymbol{u}_q \le \|\boldsymbol{K}_{pq}\|\|\boldsymbol{e}_p\| + \|\boldsymbol{K}_{dq}\|\|\dot{\boldsymbol{e}}_p\| \le K_{mq}\|\boldsymbol{q}_2\|$ and $\boldsymbol{u}_L \le \|\boldsymbol{K}_{pL}\|\|\boldsymbol{\gamma}\| + \|\boldsymbol{K}_{dL}\|\|\dot{\boldsymbol{\gamma}}\| \le K_{mL}\|\boldsymbol{q}_2\|$ where $K_{mq} = \max\{\|\boldsymbol{K}_{pq}\|, \|\boldsymbol{K}_{dq}\|\}$ and $K_{mL} = \max\{\|\boldsymbol{K}_{pL}\|, \|\boldsymbol{K}_{dL}\|\}$. Hence, based upon the above analysis, it can be derived that

$$\|\boldsymbol{h}_2\| \le (L\rho_q + \frac{1}{L}\rho_L + \rho_\gamma(\ddot{\boldsymbol{p}}_d))\|\boldsymbol{q}_2\|^2 + \bar{\rho}_\gamma(\ddot{\boldsymbol{p}}_q) \tag{72}$$

$$\|\boldsymbol{\kappa}_2\| \le \bar{g}_q\|\boldsymbol{q}_1\|f + \bar{g}_L\|\boldsymbol{q}_1\|f. \tag{73}$$

There exist two positive constants $\rho_{h2} \ge L\rho_q + \frac{1}{L}\rho_L + \rho_\gamma(\ddot{\boldsymbol{p}}_d)$ and $\rho_{\kappa_2} \ge (\bar{g}_q + \bar{g}_L)$ satisfying the following inequalities.

$$\|\boldsymbol{h}_2\| \le \rho_{h2}\|\boldsymbol{q}_2\|^2 + \bar{\rho}_\gamma \tag{74}$$

$$\|\boldsymbol{\kappa}_2\| \le \rho_{\kappa_2}f\|\boldsymbol{q}_1\| \tag{75}$$

Theorem 2: For the proposed control law in (21), (50), the quadrotor transportation system for (4)-(7) is stable, the attitude error $\|\boldsymbol{e}_R\|$ of the system converges exponentially to zero, and the position error $\|\boldsymbol{e}_p\|$ and swing angle $\|\boldsymbol{\gamma}\|$ are finally converge within a limited time for trajectory tracking.

Proof: Supposing that the matrix $\boldsymbol{A}_2$ is negative definite with all eigenvalues less than zero. The characteristic polynomial of $\boldsymbol{A}_2$ can be calculated as

$$\det(\boldsymbol{A}_2 - \lambda\boldsymbol{I}_{10}) = 0 \tag{76}$$

From (76), the conclusion that $\boldsymbol{A}_2$ is negative definite can be obtained if the control gains $\boldsymbol{K}_{pL}$, $\boldsymbol{K}_{dL}$, $\boldsymbol{K}_{pq}$, $\boldsymbol{K}_{dq}$ are positive definite and the following inequalities hold.

$$\frac{g}{L} > \frac{\lambda_3(k_{dlx} + k_{dqy})}{k_{dlx} - k_{dqx} + k_{dqy}} \tag{77}$$

$$\frac{g}{L} > \frac{\lambda_3(k_{dlx} + k_{dqy})}{k_{dlx} - k_{dqx} + k_{dqy}} \tag{78}$$

where

$$\lambda_3 = \frac{k_{dLx}k_{pqx} - k_{dqx}k_{pLy} - k_{dqx}k_{pqx} + k_{dqy}k_{pqx}}{k_{dqx}} \tag{79}$$

$$\lambda_4 = \frac{k_{dLy}k_{pqy} - k_{dqy}k_{pLx} - k_{dqy}k_{pqy} + k_{dqz}k_{pqy}}{k_{dqy}}. \tag{80}$$

Therefore, there exists a positive-definite symmetric matrix $\boldsymbol{P}_2$ satisfying the following equation.

$$\boldsymbol{A}_2^T\boldsymbol{P}_2 + \boldsymbol{P}_2\boldsymbol{A}_2 = -\boldsymbol{I}_{10} \tag{81}$$

For the dynamics of (70), a Lyapunov function is defined as

$$V_2(t) = \boldsymbol{q}_2^T\boldsymbol{P}_2\boldsymbol{q}_2. \tag{82}$$

Substituting (70) into the derivative of V yields

$$\dot{V}_2(t) = -\boldsymbol{q}_2^T\boldsymbol{q}_2 + 2\boldsymbol{q}_2^T\boldsymbol{P}_2(\boldsymbol{\kappa}_2 + \boldsymbol{h}_2). \tag{83}$$

Combining (74) and (75), the following inequality holds.

$$\dot{V}_2(t) \le -\|\boldsymbol{q}_2\|^2 + 2\rho_{h2}\|\boldsymbol{P}_2\|\|\boldsymbol{q}_2\|^3 + 2\bar{\rho}_\gamma\|\boldsymbol{P}_2\|\|\boldsymbol{q}_2\| + 2\rho_{\kappa_2}f\|\boldsymbol{P}_2\|\|\boldsymbol{q}_1\|\|\boldsymbol{q}_2\| \tag{84}$$

Based on the conditions $\|\boldsymbol{q}_2\| \le (1-\mu_h)/(2\rho_{h2}\|\boldsymbol{P}_2\|)$, $\bar{\mu}_h \ge 2\bar{\rho}_\gamma\|\boldsymbol{P}_2\|$, and $\mu_\kappa \ge 2\rho_{\kappa_2}f\|\boldsymbol{P}_2\|$, the following inequality holds.

$$\dot{V}_2(t) \le -\mu_h\|\boldsymbol{q}_2\|^2 + \bar{\mu}_h\|\boldsymbol{q}_2\| + \mu_\kappa\|\boldsymbol{q}_1\|\|\boldsymbol{q}_2\| \tag{85}$$

Define the Lyapunov function of the whole system as

$$V = \varepsilon V_1 + V_2. \tag{86}$$

Since ζ_{min} and ζ_{max} are the minimum eigenvalue and the maximum eigenvalue of $diag\{\varepsilon\boldsymbol{P}_1, \boldsymbol{P}_2\}$, $V(t)$ satisfies the following inequality.

$$\zeta_{min}\|\boldsymbol{q}\|^2 \le V \le \zeta_{max}\|\boldsymbol{q}\|^2 \tag{87}$$

Differentiating (86), and substituting (32) and (85), it follows that

$$\dot{V}(t) \le -\varepsilon\lambda_\Omega\|\boldsymbol{q}_1\|^2 - \mu_h\|\boldsymbol{q}_2\|^2 + \bar{\mu}_h\|\boldsymbol{q}_2\| + \mu_\kappa\|\boldsymbol{q}_1\|\|\boldsymbol{q}_2\|. \tag{88}$$

where $\varepsilon > \mu_\kappa/4(\mu_h - \mu) + \mu/K_\Omega$, $\mu < \varepsilon\lambda_\Omega$, and $\mu < \mu_h$. For the condition that $\ddot{\boldsymbol{p}}_d = \boldsymbol{0}$ ($\bar{\rho}_\gamma(\ddot{\boldsymbol{p}}_d) = 0$), (88) can be transformed as follow:

$$\dot{V}(t) \le -\mu\|\boldsymbol{q}\|^2. \tag{89}$$

Based upon (82) and (87), (89) is concluded as

$$\dot{V}(t) \le -\frac{2\mu}{\zeta_{max}}V(t). \tag{90}$$

The upper bound of $V(t)$ is obtained as

$$\dot{V}(t) \le V(0)\exp(-\frac{2\mu}{\zeta_{max}}t). \tag{91}$$

Then, the upper bound of $\boldsymbol{q}(t)$ is derived as

$$\|\boldsymbol{q}\| \le \sqrt{\frac{\zeta_{max}}{\zeta_{min}}}\|\boldsymbol{q}(0)\|\exp(-\frac{\mu}{\zeta_{max}}t). \tag{92}$$

Thus, for trajectory whose acceleration is zero, the system is locally exponentially stable. For the acceleration of desired trajectory is nonzero, there exists $n > 0$, satisfy

$$\dot{V}(t) \le -\mu\|\boldsymbol{q}\|^2 + \bar{\mu}_h\|\boldsymbol{q_2}\| \le -n\|\boldsymbol{q}\|^2 \tag{93}$$

with $\|\boldsymbol{q}\| \ge \frac{\bar{\mu}_h}{\mu - n}$. Thus, $\|\boldsymbol{q}\|$ is converge to a constant with exponential convergence rate.

IV. NUMERICAL SIMULATIONS AND RESULTS

This section presents the simulations to verify the control performance of the proposed control method. The contrastive analysis of the proposed controller and a sliding-mode controller (SMC) is conducted.

To verify the effectiveness of the proposed control method, we assume a quadrotor for simulations equipped with sensors that can get the measurement of the quadrotor's state as well as a motion capture system that estimates the payload's swing angle. The dynamics equations of the quadrotor suspended payload system is given by (4)-(7). And according to a quadrotor developed in [25], the model parameters are chosen as follow:

$$m_q = 1.008\ kg, \quad L = 1\ m$$
$$\boldsymbol{J} = diag([11.9, 11.9, 20.8] \times 10^{-3})\ kgm^2.$$

Based on the experiment in [39], the external disturbance is model as follow:

$$\boldsymbol{F}_e = -(\mu_1 \|\dot{\boldsymbol{p}}_q\| + \mu_2 \|\dot{\boldsymbol{p}}_q\|^2) \frac{\dot{\boldsymbol{p}}_q}{\|\dot{\boldsymbol{p}}_q\|} \tag{94}$$

where $\mu_1 = 0.172$ and $\mu_2 = 0.0025$. The proposed parameter adaptive controller is labeled as var-param controller. The SMC combined with input shaping theory and var-param controller are implemented for simulations. For the sliding-mode controller combined with input shaping theory, the position control law and the transfer function of the input shaper are as follows:

$$\boldsymbol{U} = \boldsymbol{G}_s(\ddot{\boldsymbol{p}}_{sd} - (m_q + m_p)\bar{\boldsymbol{G}} - \boldsymbol{K}\dot{\boldsymbol{q}}_s - \boldsymbol{K}_s sign(\boldsymbol{K}\boldsymbol{q}_s + \dot{\boldsymbol{q}}_s))$$
$$G = A_1 e^{t_1 s} + A_2 e^{t_2 s} + A_3 e^{t_3 s}$$

where $\boldsymbol{q}_s = \begin{bmatrix} \boldsymbol{e}_p^T & \boldsymbol{e}_R^T \end{bmatrix}^T$, $\boldsymbol{p}_{sd} = \begin{bmatrix} \boldsymbol{p}_d^T & \boldsymbol{0}_{3\times1}^T \end{bmatrix}^T$, and $\bar{\boldsymbol{G}} = \begin{bmatrix} \boldsymbol{G}^T & \boldsymbol{0}_{3\times1}^T \end{bmatrix}^T$. $\boldsymbol{K}$, $\boldsymbol{K}_s$, and $\boldsymbol{G}_s$ are the gain matrix of sliding-mode controller. A_i and t_i are the parameters of the input shaper. For our controller, the control parameters are designed in Table 2.

The simulations require the quadrotor to track the given trajectory with a payload mass of 1 kg and 0.5 kg. We consider two different trajectories including a) move from its initial position to a target position and b) a helix trajectory.

A. TRAJECTORY 1: POINT-TO-POINT CONTROL

The desire trajectory and the initial condition of the first trajectory are as follow:

$$\boldsymbol{p}_d = \begin{bmatrix} 1 & 1 & 1 \end{bmatrix}^T m, \quad \boldsymbol{b}_{1d} = \begin{bmatrix} 1 & 0 & 0 \end{bmatrix}^T$$
$$\boldsymbol{p}_0 = \begin{bmatrix} 0 & 0 & 0 \end{bmatrix}^T m, \quad \boldsymbol{R}_0 = \begin{bmatrix} 1 & 0 & 0 \\ 0 & 1 & 0 \\ 0 & 0 & 1 \end{bmatrix}.$$

The simulation results of the first trajectory are shown in Fig. 3 and Fig. 4. From Fig. 3 and Fig. 4, whatever the load mass is 0.5 kg or 1 kg, the position and the swing angle converge in 5 s by both the parameter adaptive controller and the SMC. And the steady-state position error for both

TABLE 2. Parameters of the Proposed Controller.

	var-param
$\boldsymbol{K}_{pq}$	$diag([1, 1, 6])$
$\boldsymbol{K}_{dq}$	$diag([0.6(5 - m_p), 0.6(5 - m_p), 7])$
$\boldsymbol{K}_{pL}$	$diag([16m_p/5, 16m_p/5])$
$\boldsymbol{K}_{dL}$	$diag([2m_p, 2m_p])$
k_m	$1/3$

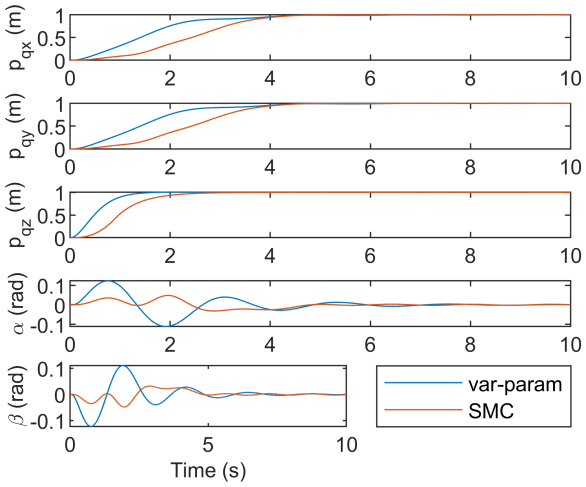

(a) position and swing angle.

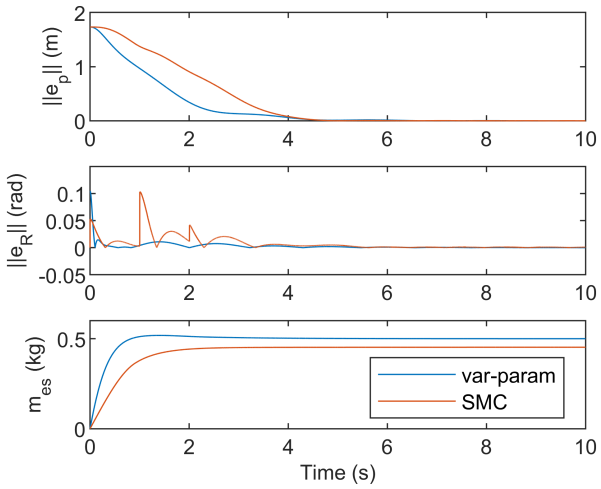

(b) position error and attitude error.

FIGURE 3. Results of quadrotor with payload mass of 0.5 kg in the first trajectory.

two controllers are smaller than 0.002 m. For the steady-state error, the estimated mass of the var-param controller is smaller than that of the SMC. Although the swing angle of the var-param controller is larger than that of the SMC, the attitude error and position error of the parameter adaptive controller have smaller oscillation regardless of the load mass of 0.5kg or 1kg. In addition, SMC shows more dramatic oscillations of the z-axis position with the payload mass of 1 kg in Fig. 4. Hence, for point-to-point flight, both two controllers deliver good performance under environmental perturbation, but the parameter adaptive controller induces more robust effects than SMC for unknown mass.

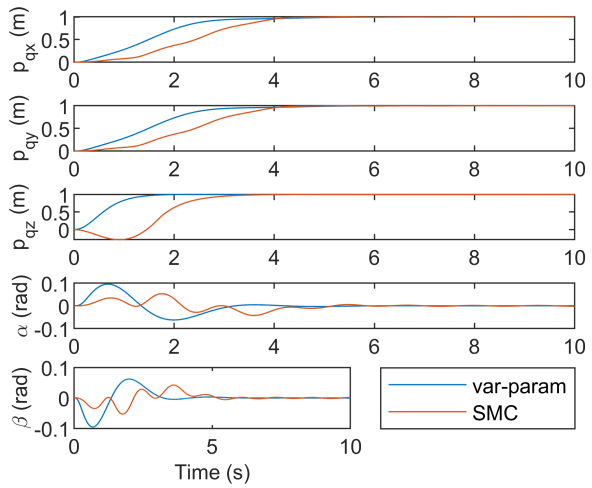

(a) position and swing angle.

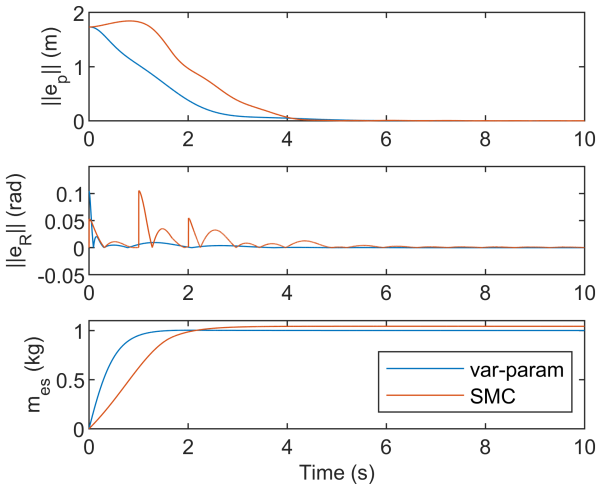

(b) position error and attitude error.

FIGURE 4. Results of quadrotor with payload mass of 1 kg in the first trajectory.

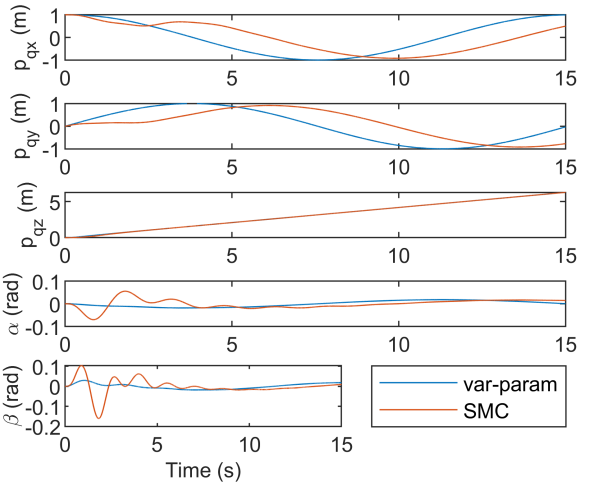

(a) position and swing angle.

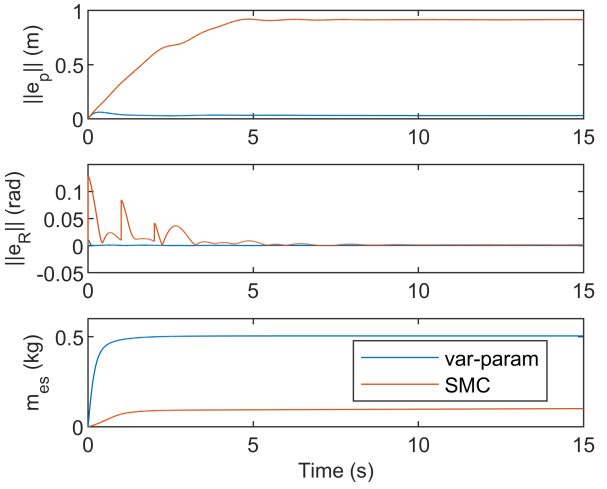

(b) position error and attitude error.

FIGURE 5. Results of quadrotor with payload mass of 0.5 kg in the second trajectory.

B. TRAJECTORY 2: TRACKING CONTROL

The acceleration of the second given trajectory is nonzero. The desired trajectory and the initial condition of the system are set as:

$$\boldsymbol{p}_d = \begin{bmatrix}\cos(0.3t) & \sin(0.3t) & 0.3t\end{bmatrix}^T m, \quad \boldsymbol{b}_{1d} = \begin{bmatrix}1 & 0 & 0\end{bmatrix}^T$$

$$\boldsymbol{p}_0 = \begin{bmatrix}1 & 0 & 0\end{bmatrix}^T m, \quad \boldsymbol{R}_d = \begin{bmatrix}1 & 0 & 0\\ 0 & 1 & 0\\ 0 & 0 & 1\end{bmatrix}.$$

The simulation results of the second trajectory are shown in Fig. 5 and Fig. 6. From Fig. 5 and Fig. 6, at a payload mass of both 0.5 kg and 1 kg, the position error, attitude error, and the swing angle for the var-param controller converge within 5 s. For the steady state, the error of the var-param controller on position, attitude, and estimated mass are all less than that of SMC. Furthermore, for the var-param controller, the response curves of position error, attitude error, and swing angle are smoother. In Fig. 6, SMC shows more dramatic oscillations on the z-axis position when payload mass is 1 kg. As a result, for trajectory tracking flight, the var-param controller achieves better performance than SMC when subjected to unknown mass and air disturbance.

C. PERFORMANCE MEASURES

In addition, refer to the method proposed in [24], we conduct a comparative analysis for position error and swing angle of the var-param control system and the sliding-mode control system. The performance comparison for integrated absolute error (IAE) of two controllers performance is define as follow:

$$\eta = \frac{\int |e_{var}|dt}{\int |e_{smc}|dt} \tag{95}$$

where e_{var} and e_{smc} represent the errors of the var-param controller and the SMC. After that calculations, the performance indexes are concluded in Table 3.

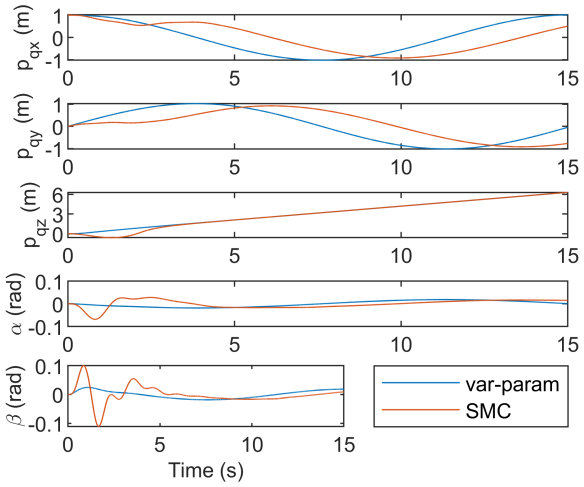

(a) position and swing angle.

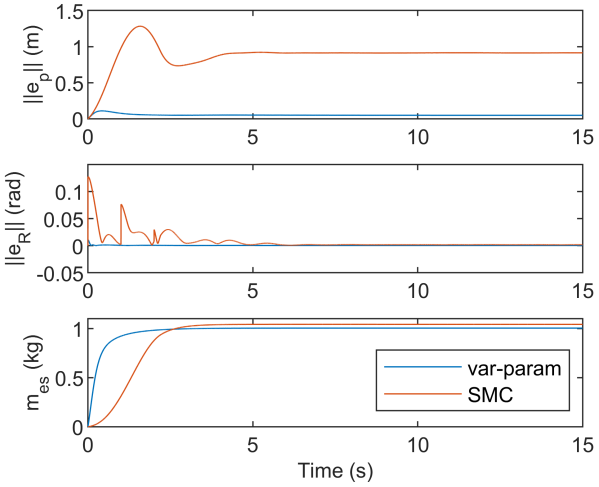

(b) position error and attitude error.

FIGURE 6. Results of quadrotor with payload mass of 1 kg in the second trajectory.

TABLE 3. Performance Index of Two Controllers.

	$\ddot{\boldsymbol{p}}_d = \mathbf{0}$		$\ddot{\boldsymbol{p}}_d \neq \mathbf{0}$	
	$0.5\ kg$	$1\ kg$	$0.5\ kg$	$1\ kg$
η_x	0.65	0.67	0.04	0.06
η_y	0.65	0.67	0.03	0.06
η_z	0.51	0.29	0.39	0.07
η_α	2.30	1.38	0.52	0.63
η_β	2.30	1.39	0.74	0.79

In Table 3, η_x, η_y, and η_z represent the performance of the controllers in x-axis, y-axis, and z-axis of position. η_α and η_β represent the performance of the controllers in swing angle. η performance criteria is defined as follows. If the η is less than 1, it means that the error of the var-param controller is smaller. Also, if this η is greater than 1, it indicates that the performance of the var-param controller is poorer than the SMC.

From Table 3, for the flight to a target position, although the swing angle of the var-param controller is larger than that of the SMC, the var-param controller indicates better performance on position control, specifically the z-axis position. With the trajectory whose accelerate is nonzero, the parameter adaptive controller has a very good effect in position control with good suppression of swing. Hence, it can be concluded that the parameter adaptive controller improves the performance of trajectory tracking control compared to the SMC when facing unknown mass and air disturbance.

V. CONCLUSION

In this paper, a novel control method with anti-disturbance capability is presented to quickly track trajectory for a quadrotor transporting a suspended payload. First, based on linear feedback and estimated payload mass, the parameter adaptive control system is designed for position control and swing suppression. In addition, we add a mass estimation algorithm to the parameter adaptive controller for stable control under unknown mass and varying mass in the air. The simulations corresponding to different payload mass and two different trajectories are carried on. Simulation results demonstrate that the parameter adaptive controller is greatly superior to the SMC controller under unknown mass and air disturbance, with a maximum payload mass of up to 1kg.

The contribution of this work is improving the tracking accuracy for the quadrotor with a suspended payload under large unknown load and air disturbance conditions. With this control method, the robustness and load-bearing capacity of a quadrotor transportation system are substantially enhanced. This is an important difference from most methods that require known payload mass to achieve stable control. The future work will focus on the control of multiple quadrotors with a suspended payload and expansion of this work to outdoor experiments.

REFERENCES

[1] V. Roberge, M. Tarbouchi, and G. Labonté, "Fast genetic algorithm path planner for fixed-wing military UAV using GPU," *IEEE Trans. Aerosp. Electron. Syst.*, vol. 54, no. 5, pp. 2105–2117, Oct. 2018.

[2] Y. Mualla, A. Najjar, A. Daoud, S. Galland, C. Nicolle, A.-U.-H. Yasar, and E. Shakshuki, "Agent-based simulation of unmanned aerial vehicles in civilian applications: A systematic literature review and research directions," *Future Gener. Comput. Syst.*, vol. 100, pp. 344–364, Nov. 2019.

[3] H. Qiu and H. Duan, "A multi-objective pigeon-inspired optimization approach to UAV distributed flocking among obstacles," *Inf. Sci.*, vol. 509, pp. 515–529, Jan. 2020.

[4] S. Mallavalli and A. Fekih, "A fault tolerant tracking control for a quadrotor UAV subject to simultaneous actuator faults and exogenous disturbances," *Int. J. Control*, vol. 93, no. 3, pp. 655–668, 2020.

[5] M. E. Guerrero-Sánchez, D. A. Mercado-Ravell, R. Lozano, and C. D. García-Beltrán, "Swing-attenuation for a quadrotor transporting a cable-suspended payload," *ISA Trans.*, vol. 68, pp. 433–449, May 2017.

[6] D. Giles and R. Billing, "Deployment and performance of a UAV for crop spraying," *Chem. Eng. Trans.*, vol. 44, pp. 307–312, Oct. 2015.

[7] H. Huang and A. V. Savkin, "An algorithm of reactive collision free 3-D deployment of networked unmanned aerial vehicles for surveillance and monitoring," *IEEE Trans. Ind. Informat.*, vol. 16, no. 1, pp. 132–140, Jan. 2020.

[8] H. X. Pham, H. M. La, D. Feil-Seifer, and M. C. Deans, "A distributed control framework of multiple unmanned aerial vehicles for dynamic wildfire tracking," *IEEE Trans. Syst., Man, Cybern. Syst.*, vol. 50, no. 4, pp. 1537–1548, Apr. 2020.

[9] B. D. Song, K. Park, and J. Kim, "Persistent UAV delivery logistics: MILP formulation and efficient heuristic," *Comput. Ind. Eng.*, vol. 120, pp. 418–428, Jun. 2018.

[10] E. Ackerman and E. Strickland, "Medical delivery drones take flight in East Africa," *IEEE Spectr.*, vol. 55, no. 1, pp. 34–35, Jan. 2018.

[11] P. J. Cruz and R. Fierro, "Cable-suspended load lifting by a quadrotor UAV: Hybrid model, trajectory generation, and control," *Auto. Robots*, vol. 41, no. 8, pp. 1629–1643, Dec. 2017.

[12] S. Tang and V. Kumar, "Mixed integer quadratic program trajectory generation for a quadrotor with a cable-suspended payload," in *Proc. IEEE Int. Conf. Robot. Autom. (ICRA)*, May 2015, pp. 2216–2222.

[13] M. Orsag, C. Korpela, and P. Oh, "Modeling and control of MM-UAV: Mobile manipulating unmanned aerial vehicle," *J. Intell., Robotic Syst.*, vol. 69, nos. 1–4, pp. 227–240, 2013.

[14] T. Wang, K. Umemoto, T. Endo, and F. Matsuno, "Modeling and control of a quadrotor UAV equipped with a flexible arm in vertical plane," *IEEE Access*, vol. 9, pp. 98476–98489, 2021.

[15] X. Liang and Y. Hu, "Tracking control and differential flatness of quadrotor with cable-suspended load," in *Proc. IEEE 3rd Inf. Technol., Netw., Electron. Autom. Control Conf. (ITNEC)*, Mar. 2019, pp. 88–92.

[16] K. P. Valavanis and G. J. Vachtsevanos, "Modeling of a micro UAV with slung payload," in *Handbook of Unmanned Aerial Vehicles*. Dordrecht, The Netherlands: Springer, 2015, pp. 1257–1272.

[17] C. Wu, Z. Fu, J. Yang, and Y. Wei, "Nonlinear control and analysis of a quadrotor with sling load in path tracking," in *Proc. 36th Chin. Control Conf. (CCC)*, Jul. 2017, pp. 6519–6524.

[18] S. Sadr, S. A. A. Moosavian, and P. Zarafshan, "Dynamics modeling and control of a quadrotor with swing load," *J. Robot.*, vol. 2014, pp. 1–12, Dec. 2014.

[19] I. Palunko, R. Fierro, and P. Cruz, "Trajectory generation for swing-free maneuvers of a quadrotor with suspended payload: A dynamic programming approach," in *Proc. IEEE Int. Conf. Robot. Autom.*, May 2012, pp. 2691–2697.

[20] J. Su, J.-H. Bak, and J. Hyun, "Optimal trajectory generation for quadrotor with suspended load under swing angle constraint," in *Proc. IEEE 15th Int. Conf. Control Autom. (ICCA)*, Jul. 2019, pp. 549–554.

[21] B. Xian, S. Wang, and S. Yang, "Nonlinear adaptive control for an unmanned aerial payload transportation system: Theory and experimental validation," *Nonlinear Dyn.*, vol. 98, no. 3, pp. 1745–1760, Nov. 2019.

[22] M. E. Guerrero-Sánchez, R. Lozano, P. Castillo, O. Hernández-González, C. D. García-Beltrán, and G. Valencia-Palomo, "Nonlinear control strategies for a UAV carrying a load with swing attenuation," *Appl. Math. Model.*, vol. 91, pp. 709–722, Mar. 2021.

[23] K. Klausen, T. I. Fossen, and T. A. Johansen, "Nonlinear control with swing damping of a multirotor UAV with suspended load," *J. Intell. Robotic Syst.*, vol. 88, nos. 2–4, pp. 379–394, 2017.

[24] K. Y. Us, A. Cevher, M. Sever, and A. Kırlı, "On the effect of slung load on quadrotor performance," *Proc. Comput. Sci.*, vol. 158, pp. 346–354, Jan. 2019.

[25] S. Yang and B. Xian, "Exponential regulation control of a quadrotor unmanned aerial vehicle with a suspended payload," *IEEE Trans. Control Syst. Technol.*, vol. 28, no. 6, pp. 2762–2769, Nov. 2020.

[26] D. Cabecinhas, R. Cunha, and C. Silvestre, "A trajectory tracking control law for a quadrotor with slung load," *Automatica*, vol. 106, pp. 384–389, Aug. 2019.

[27] T. Kusznir and J. Smoczek, "Sliding mode-based control of a UAV quadrotor for suppressing the cable-suspended payload vibration," *J. Control Sci. Eng.*, vol. 2020, pp. 1–12, 2020, doi: 10.1155/2020/5058039.

[28] M. Bisheban and T. Lee, "Computational geometric identification for quadrotor dynamics in wind fields," in *Proc. IEEE Conf. Control Technol. Appl. (CCTA)*, Aug. 2017, pp. 1153–1158.

[29] B. Zhu, Q. Zhang, and H. H.-T. Liu, "A comparative study of robust attitude synchronization controllers for multiple 3-DOF helicopters," in *Proc. Amer. Control Conf. (ACC)*, Jul. 2015, pp. 5960–5965.

[30] L. Qian and H. H. T. Liu, "Path-following control of a quadrotor UAV with a cable-suspended payload under wind disturbances," *IEEE Trans. Ind. Electron.*, vol. 67, no. 3, pp. 2021–2029, Mar. 2020.

[31] V. S. Deshpande and S. B. Phadke, "Control of uncertain nonlinear systems using an uncertainty and disturbance estimator," *J. Dyn. Syst., Meas., Control*, vol. 134, no. 2, pp. 1–7, Mar. 2012.

[32] K. Guo, J. Jia, X. Yu, L. Guo, and L. Xie, "Multiple observers based anti-disturbance control for a quadrotor UAV against payload and wind disturbances," *Control Eng. Pract.*, vol. 102, Sep. 2020, Art. no. 104560, doi: 10.1016/j.conengprac.2020.104560.

[33] K. Eliker, S. Grouni, M. Tadjine, and W. Zhang, "Practical finite time adaptive robust flight control system for quad-copter UAVs," *Aerosp. Sci. Technol.*, vol. 98, Mar. 2020, Art. no. 105708, doi: 10.1016/j.ast.2020.105708.

[34] O. Mofid, S. Mobayen, and W.-K. Wong, "Adaptive terminal sliding mode control for attitude and position tracking control of quadrotor UAVs in the existence of external disturbance," *IEEE Access*, vol. 9, pp. 3428–3440, 2021.

[35] A. Roberts and A. Tayebi, "Adaptive position tracking of VTOL UAVs," *IEEE Trans. Robot.*, vol. 27, no. 1, pp. 129–142, Feb. 2011.

[36] P. E. I. Pounds, D. R. Bersak, and A. M. Dollár, "Stability of small-scale UAV helicopters and quadrotors with added payload mass under PID control," *Auton. Robots*, vol. 33, nos. 1–2, pp. 129–142, 2012.

[37] Z. Liu, X. Liu, J. Cheng, and C. Fang, "Altitude control for variable load quadrotor via learning rate based robust sliding mode controller," *IEEE Access*, vol. 7, pp. 9736–9744, 2019.

[38] S. Dai, T. Lee, and D. S. Bernstein, "Adaptive control of a quadrotor UAV transporting a cable-suspended load with unknown mass," in *Proc. 53rd IEEE Conf. Decis. Control*, Dec. 2014, pp. 6149–6154.

[39] M. Schulz, F. Augugliaro, R. Ritz, and R. D'Andrea, "High-speed, steady flight with a quadrocopter in a confined environment using a tether," in *Proc. IEEE/RSJ Int. Conf. Intell. Robots Syst. (IROS)*, Sep. 2015, pp. 1279–1284.

YING WU was born in Guangzhou, Guangdong, China, in 1997. She received the B.Eng. degree in automation from the Guangdong University of Technology, Guangzhou, in 2019, where she is currently pursuing the M.Eng. degree in control science and engineering. Her main research interests include control systems, trajectory planning, and robotics applications.

YUN XIE was born in 1964. She received the B.S. and M.S. degrees in radio from Jiangxi University, Jiangxi, China, in 1985 and 1990, the M.S. degree in radio from Peking University, Beijing, China, in 1991, and the Ph.D. degree in mechanical engineering from the Guangdong University of Technology, Guangzhou, China, in 2005. She was a Visiting Scholar with the University of Nantes, France, in 2007, and the University of California at San Diego, San Diego, CA, USA, in 2014. She is currently a Professor with the Guangdong University of Technology. She is the author of more than 80 articles. Her research interests include electronic information, intelligent robotics, and brain–computer interface.

SEN LI received the B.Eng. degree in electronic engineering from the Guangdong University of Technology, Guangzhou, Guangdong, China, in 2019, where he is currently pursuing the M.Eng. degree in control science and engineering with the Jet Power and Humanoid Robotics Laboratory. His research interests include biomimetic strategies, dynamics, control, and algorithmic applications.